

Convective Boiling in Metallic Foam: Experimental Analysis of the Pressure Loss

B. Madani¹, F. Topin² and L. Tadrist²

Abstract: The present work deals with the hydraulic characterization of two-phase flow with phase change in a channel filled with metallic foam. We provide a general presentation of metallic foams including morphological characteristics, fabrication processes and industrial applications. The experimental facility, which consists of a hydrodynamic loop, the test section, measurement devices, and the data acquisition system, is presented. The Metallic foam sample tested in the present work is manufactured by SCPS (French manufacturer). N-pentane is used as a coolant fluid. The mass velocity values lie between 4 and 49 kg/ m²s, while the heating power in the test section ranges from 0 to 35 W/cm². The effect of fluid acceleration on the pressure profiles is demonstrated in the convective boiling regime. The measured pressure profiles are used to locate the thermodynamic zones inside the test channel. Then, the evolution of the pressure drop versus mass velocity is established and compared to results obtained from the application of the homogeneous model to two-phase flow.

Keywords: Two-phase flow, boiling, pressure loss, homogeneous model, multiplier parameter.

1 Introduction

Metallic foams are a class of cellular materials elaborated from either liquid or metallic powder. The foam utilized in this study is obtained by electro-deposition process. An exhaustive review about processes used to elaborate metallic foam is given by Curran (2003). As shown in Fig. 1, the geometric structure of metallic foam is constituted of fluid cells with polyhedron shape. Each cell is delimited by struts, with roughly triangular hollowed section. The number of pores by inch (PPI) is generally used by manufacturers to characterize the material pore size.

¹ Corresponding author: LTPMP, FGMGP, USTHB, Algiers, Algeria, Email: bmadani@usthb.dz.

² IUSTI, U. Provence, Marseille, France.

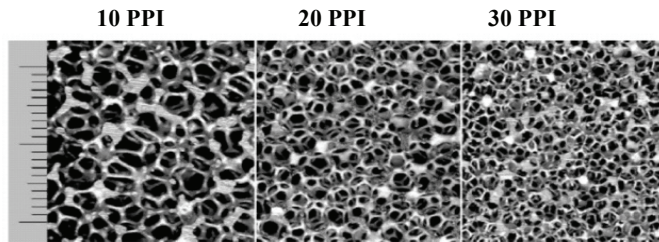


Figure 1: Metallic foams for three different ppi.

Initially, metallic foams were used in aeronautic and transportation vehicles due to their mechanical properties such as strength and choc absorption. Only during the last decade have the thermal applications begun to be developed. Nowadays, open cell metallic foams are widely used in heat and mass transfer enhancement such as in catalyst exchangers.

In the literature, a large number of studies concerning the thermo-hydraulic characterization of metallic foam were carried out in the single-phase regime (liquid or gas) (Kaviany and Mittal, 1987; Bhattacharya, Calmidi and Mahajan, 2002; Boomsma and Poulikakos, 2002; Tadrst, Miscevic, Rahli and Topin, 2004; Madani, Topin, Rigollet and Tadrst, 2007; Mahjoob and Vafai, 2008; Bonnet, Topin and Tadrst, 2008). There are a few studies on two-phase flow in fibrous media and metallic foam (Miscevic, Topin and Tadrst, 2002; Topin, Bonnet, Madani and Tadrst, 2006; Stemmet, Jongmans, Schaaf, Kuster, and Schouten, 2005; Calvo, Beugre, Crine, Léonard, Marchot, and Toye, 2009). There is also a lot of work dealing with two-phase and boiling in porous media (Lipinski, 1980; Bau and Torrance, 1982; Naik and Dhir, 1982; Nakayama, Daikoku and Nakajima, 1982; Fukusako, Komoriya and Seki, 1986; Kovalev, Solov'yev and Ovodkov, 1987; Chung and Catton, 1988; Kaviany, 1991; Carey, 1992; Liao and Zhao, 2000; Jamialahmadi, Müller-Steinhagen and Izadpanah, 2005). Madani (2007) gives an exhaustive review on boiling in porous media as well as its everyday applications in nature and in industrial activities.

The hydraulic properties of the foam used in the present work may be found in Madani, Topin, Rigollet and Tadrst (2007).

2 Experimental Facilities

The experimental set-up is designed to allow the study of the impact of a solid matrix on the flow and the heat transfer phenomena in either single-phase or boil-

ing regime. The apparatus (Fig. 2) consists of three main parts: a test section, a fluid loop and a data acquisition system. The test section is a rectangular channel containing metallic foam. The foams used in the present study and shown on the photo in Fig. 3 are manufactured by SCPS (1995, 1998) via electro-deposition and shaped as plates of 3 to 7 mm thickness. Image analysis was used to determine the geometric characteristics of this metallic foam. The grade and the average diameter pore size are 36 PPI (pore per linear inch) and 0.6 mm respectively. Note that the grade provided by the manufacturer is 40 PPI. However, the porosity given by the manufacturer, which is equal to 95%, is the same as the one measured in-situ by weighting. The channel is encapsulated in a PTFE (PolyTetraFluoroEthylene) box, ensuring both mechanical tightness and thermal insulation.

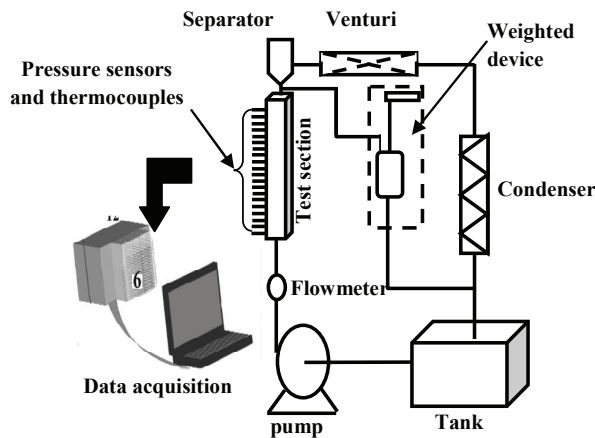


Figure 2: Experimental set-up for boiling experiments

The test section shown in Fig. 4-a, is a channel with dimensions 10 mm (W) x 50 mm (L) x 200 mm (H), which contains foam plates that are not soldered to the heating plates. The test section is heated on both lateral surfaces using electric heaters. The channel is provided with forty thermocouples (type K) with diameter equal to 0.5 mm and an approximate sensitivity of $41 \mp \mu\text{V}/^\circ\text{C}$. These thermocouples are placed in the wall and inside the metallic foam along the three vertical axes: wall temperatures ($x=-0.01\text{cm}$), axial temperatures ($x=0.5\text{cm}$) and middle metallic foam sample temperature ($x=0.25\text{cm}$). Notice that the x reference axis is on the internal side of the channel wall as shown in Fig. 4-b.

Pressure is measured using Sensym pressure transducers which are attached to needles ($d=0.5\text{mm}$) and located in the foam and uniformly spaced 10 mm apart along

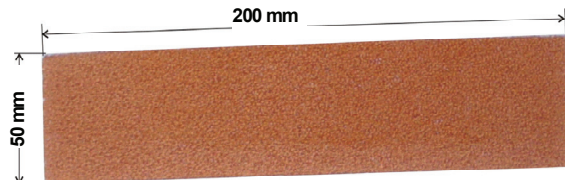


Figure 3: Plate of SCPS metallic foam made up of copper, with 36 PPI as grade, 95% porosity, $D_{pore}=0.7$ mm, $D_{strut}=0.178$ mm.

the central axis (Fig. 4-b). The sensors' range is from 0 to 1.03 bar and their sensitivity is about $1.7\mu\text{V}/\text{Pa}$.

The fluid loop consists of a storage tank, a variable velocity gear pump and a cryostat for the control of the inlet liquid temperature (i.e. n-pentane).

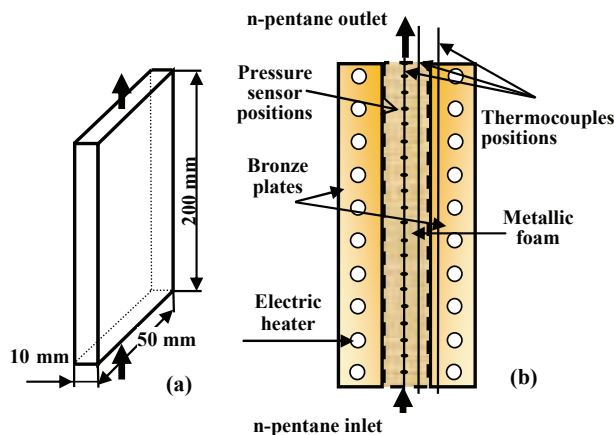


Figure 4: The test section: (a) Channel dimension, (b) Channel components

The test section is connected downstream to a separator which is used only for two-phase flow experiments. The liquid flows down by gravity to the weighted tank, which is used to assess the mass flow rate, and eventually to the storage tank. The constraint gauge which is the main element of the balance was calibrated in the range 0 to 3 kg with a sensitivity of $7.5\mu\text{V}/\text{g}$. The inlet test section flow rate is monitored using two turbines flowmeters for optimal accuracy over the full range of experiments. The first flowmeter works between 0.2 l/mn and 2 l/mn with a

sensitivity of 2.5 V for 1l/mn, while the second covers the range from 1l/mn to 40l/mn with a sensitivity equal to 1.2V for 1 l/mn. The measurement of liquid mass flow rate both upstream the test section and coming to the weighted tank allows the determination of the exit mass vapor quality.

Note that the heating power and the exit mass quality have also been calculated using an energy balance. The discrepancy between the calculated and the measured quantities is less than 2% for heating power and 7% for exit mass quality.

3 Experimental results and discussion

3.1 Pressure loss measurements

The pressure profiles measured along the foam are shown in Fig. 5 for five various of the flow rate and a constant heating power $P= 4228\text{W}$. The measured exit mass quality is also reported for each flow rate.

Although twenty sensors are implanted along the channel's central axis (see in Fig. 4-b), measurements of the pressure are provided at only thirteen locations. This is due to the fact that the sensors in the omitted positions gave useless responses.

In Fig. 5, we can easily see that the total pressure loss increases with inlet fluid velocity. On the other hand, all the curves present two distinct parts: the first part is linear, near the channel entrance, while the second is quadratic, extending to the channel exit. Notice that the first part of curves presented in Fig. 5 corresponds to the single-phase (liquid) flow regime and the second to the two-phase flow regime.

The slopes of the five curves in the single-phase zone are nearly identical. This result is similar than that obtained by Madani (2007) in their single-phase hydraulic characterization of the present metallic foam samples. In fact, in the $[20- 50]$ $\text{kg/m}^2\text{s}$ range of mass velocity with no heating power, the pressure profile slopes were found identical within the uncertainty of the experiments in the cited work. The authors used a larger mass velocity range between 6 and 122 $\text{kg/m}^2\text{s}$ to determine both the inertial and the viscous contributions. The results, which are based on a parameter estimation method, show the predominance of the inertial character of the flow in this type of cellular material. In the second part of the curves, the pressure gradient increase indicates that the mixture density variation effect is not negligible here. This density variation is produced by both phase change and gas compressibility effects. Thus, the mixture velocity should increase from the inlet to outlet, producing an increasing in pressure gradient. Figure 5 also shows that the increase in mass velocity increases the pressure profile curvature and so the pressure gradient. Notice that this last parameter increases rapidly near the exit channel.

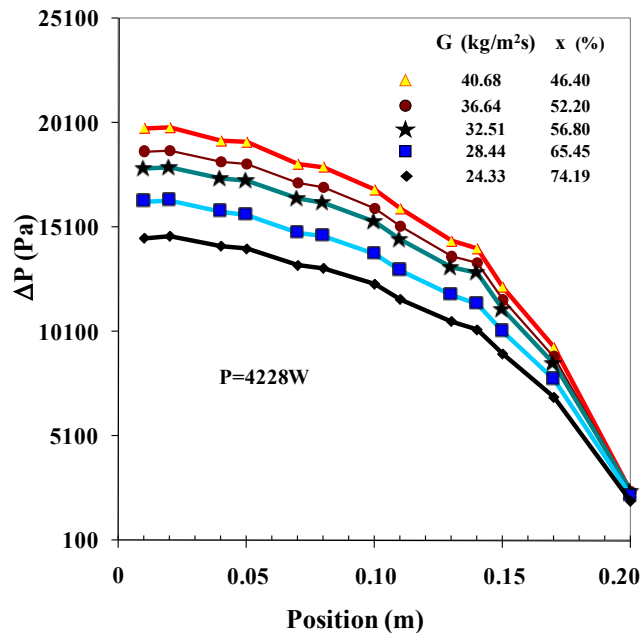


Figure 5: Local static pressure profiles along the channel for several liquid mass velocities and heating power $P=4228\text{W}$. The exit mass quality is given for each mass velocity.

Figure 5 clearly shows that the pressure gradient is less in the single-phase region than in the two-phase region.

3.2 Convective boiling flow laws

Experimental results for the pressure gradient are given in Fig. 6 for several heating power values. The pressure gradient increases with both heating power and mass velocity. This phenomenon may be explained by the fact that for a high heating power, the boiling regime in the channel is stronger, so that more and more nucleate sites are activated on both the channel walls and the solid matrix. The generated bubbles coalesce to form slugs.

For visualisation purposes, a special test section has been set up with one of the metallic plates replaced by a glass sheet. More details about this device are given in Topin, Bonnet, Madani and Tadrist (2006). This special facility, which is equipped with a fast camera, allows taking surface photos of the convective boiling in our foams. These photos show that the slugs generated by boiling cling to the walls and obstruct momentarily the matrix pores, resulting in a high pressure at the entrance

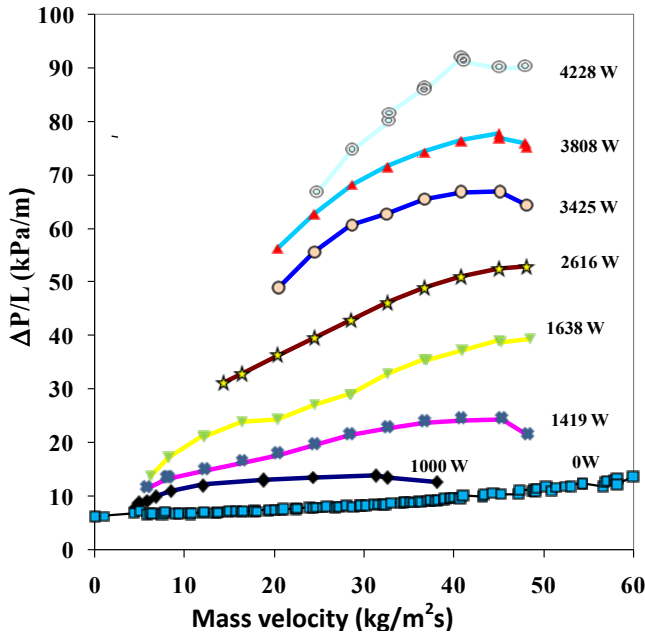


Figure 6: Pressure gradient *versus* mass velocity for several heating power values: experimental results.

part of the channel. Moreover, each curve has a maximum point past which, the curves converge to the single-phase regime curve. At this maximum, the mass velocity is so high that the applied heat power is fully absorbed to heat up the liquid. Consequently there is no enough energy to maintain the boiling regime. However, we note that the starting point of 1000W, 1419W and 1638W curves converge to the single-phase curve. This means that these points indicate the beginning of the liquid phase disappearance, or in other words that to the left of these working points the flow in the channel is a single-phase gas.

3.3 Hydraulic modelling of convective boiling

In the literature, there are neither experimental results for boiling in metallic foam nor agreement on a two-phase flow model for porous media. Thus, in order to compare our experimental results with reference cases, and considering the very high porosity of the metallic foam which is close to 95%, we decided to compare them to the results obtained with the homogeneous model for two-phase flow in a clear tube. Among the advantages offered by this model, the specific velocities of each phase which are missing in our database, are not requested.

Recall that the homogeneous model is a set of equations expressing conservation of mass and momentum. In this model, two-phase flow is considered as a single-phase flow possessing mean properties. In addition, the vapor and liquid are assumed to have the same velocity. Consequently, the local two-phase flow configuration is not taken into account; more details can be found in Herstroni (1982).

In the following formulation, 1D geometric configuration and steady state are assumed. These assumptions are justified by the channel dimensions and the experimental conditions.

Globally for the two-phase flow, the total static pressure loss is the sum of a friction, an acceleration and gravity term (Eq. 1).

$$\Delta P_{total} = \Delta P_{friction} + \Delta P_{acceleration} + \Delta P_{gravity} \quad (1)$$

In Collier (1972), the expressions for the various components have been obtained using a simplified one-dimension analysis for the two-phase flow in an inclined duct. In that analysis, the considered duct is separated by a plane parallel to the axis into upper vapor and lower liquid parts. The frictional component of the total pressure drop in this formulation is expressed in terms of the single-phase liquid pressure gradient $\left(\frac{\partial P}{\partial z}\right)_{LO}$ and the two-phase homogeneous multiplier ϕ_{LO}^2 as given in Eq.2.

$$\left(\frac{\partial P}{\partial z}\right)_F = \phi_{LO}^2 \left(\frac{\partial P}{\partial z}\right)_{LO} \quad (2)$$

For a turbulent flow regime ϕ_{LO}^2 is given by Eq.3.

$$\phi_{LO}^2 = \left(1 + x \frac{\rho_L - \rho_G}{\rho_G}\right) \left(1 + x \frac{\mu_L - \mu_G}{\mu_G}\right)^{-1/4} \quad (3)$$

Where x represents the mass quality, ρ [kg/m³] the density and μ [Ns/m²] the viscosity.

The single-phase liquid flow pressure drop is determined using Forchheimer's formula (Eq. 4).

$$\left(\frac{dP}{dz}\right)_{LO} = \alpha U + \beta U^2 \quad (4)$$

Both the viscous parameter α [Pa s/m²] and the inertial parameter β [kg/m⁴] have previously been determined by Madani, Topin, Rigolet and Tadrist (2007) in their

experimental work about the single-phase flow laws in metallic foams. In the above equation, U is the superficial velocity [m/s] of the single-phase flow.

The acceleration and gravity components are given by Eqs 5 and 6, respectively.

$$\left(\frac{dP}{dz}\right)_a = G \frac{d\bar{u}}{dz} = G^2 \frac{d\bar{v}}{dz} = G^2 \frac{d}{dz} \left[\frac{(1-x)^2 v_f}{(1-\alpha)} + \frac{x^2 v_g}{\alpha} \right] \quad (5)$$

$$\left(\frac{dP}{dz}\right)_g = \bar{\rho} g \sin \theta = [(1-\alpha)\rho_f + \alpha\rho_g] g \sin \theta \quad (6)$$

In the above equations, G is the inlet mass velocity [$\text{kg}/\text{m}^2\text{s}$], while \bar{u} [m/s], \bar{v} [m^3/kg] and $\bar{\rho}$ [kg/m^3] stand for the average value of velocity, specific volume and density of the homogeneous fluid, respectively. The inclination of the duct is θ . The subscript f denotes the liquid phase and g the vapor phase. The void fraction α is given by Eq.7.

$$\alpha = \frac{x}{x + S(1-x)\frac{\rho_g}{\rho_f}} \text{ with } S = \frac{u_g}{u_f} \quad (7)$$

In this formula S is the slip ratio, u_f and u_g being the actual velocities of the liquid and vapor phases, respectively. For the particular case of the homogeneous model, S is taken equal to unity since $u_g = u_f = \bar{u}$.

As mentioned previously, the facilities used in the present work do not provide access to mass vapor quality along the channel and that's why a profile for this parameter must be adopted and wedged on the exit quality value. Obviously, the linear profile is the simplest one that we can utilize here. Consider the channel inlet at the z -axis origin. Then, expression of mass quality function z is given by Eq.8.

$$x = \frac{z - z_{dz}}{L_{dz}} x_{out} \quad (8)$$

Where x is the mass quality at position z , z_{dz} the beginning position of the two-phase zone, x_{out} the channel exit mass quality and L_{dz} the length of the two-phase zone.

Consider a constant heat flux distribution along the channel walls, an assumption which is widely used in Heat Transfer Modelling. Equation 9 gives the exit mass quality of an element (i) located in the two-phase flow zone in terms of position and heat flux.

$$x_{i+1} = x_i + (z_{i+1} - z_i) \frac{Q\Pi}{GAh_{LG}} \quad (9)$$

In this expression \dot{Q} [W/m²] is the heat flux, Π [m], A [m²], G [kg/m²s] and h_{LG} [J/kg] being the perimeter, the straight section of the channel, the mass flux and the latent heat, respectively. The subscripts i and $i+1$ refer to the inlet and the outlet of the element considered.

The total pressure drop and its components (friction, acceleration and gravity) *versus* position z are illustrated in Fig. 7. The results are obtained for a heating power $P= 1637\text{W}$, a mass velocity $G= 24 \text{ kg/m}^2\text{s}$, a length of the two-phase flow $L_{tp}= 0.12\text{m}$ and an exit mass quality $x=24\%$.

As expected, the Fig. 7 shows that the friction component dominates the total pressure drop. In this case, the friction pressure drop along the two-phase zone of the channel represents 80% of the total pressure drop, the acceleration 18% and the gravity 2%.

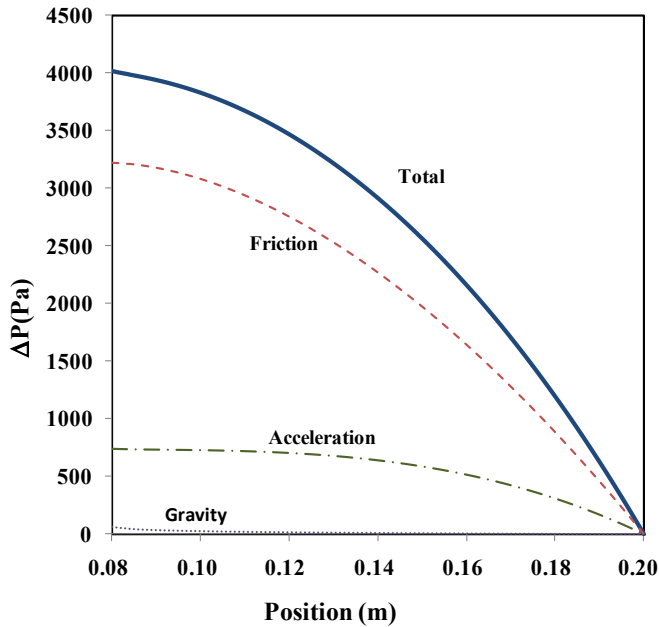


Figure 7: Total pressure drop and its components (friction, acceleration and gravity) for heating power $P= 1637\text{W}$, mass velocity $G=24 \text{ kg/m}^2$ and exit mass quality $x= 24\%$.

The plot of two-phase homogeneous multiplier parameter *versus* mass quality is given in Fig. 8, which is built using Eq. 3 for the turbulent flow. The ratio ξ_{LO}^2 of the two-phase total pressure drop to the single-phase pressure drop for all boiling

experimental results are also presented in Fig. 8.

Recall that for these experiments, the boiling power ranges from 5 to 35 (W/cm²) while the mass velocity is in the range [4-49] (kg/m²s). As we can see, the experimental points follow well the shape of the multiplier parameter curve and are globally gathered in a narrow band closer to this curve. On the one hand, this result confirms the predominance of the friction pressure drop in the expression of the total pressure drop as shown in Fig. 7. On the other hand, the figure shows that the friction pressure loss, as given by the model, is overestimated. As can be seen, several mass quality values are related to more than one ratio ξ_{LO}^2 . This fact is due in particular to the possibility that one mass quality can be obtained for several mass velocities.

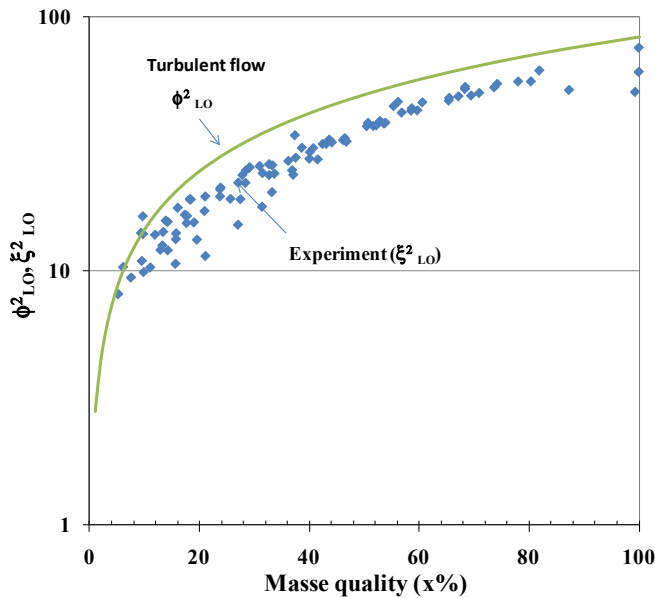


Figure 8: Homogeneous multiplier parameter *versus* mass quality compared to ratio of two- phase total pressure loss to single-phase pressure loss.

The curves shown in Fig. 9 compare the modeling results with experiment, in terms of total pressure loss along the channel for several heating power values and a constant mass velocity of 24 kg/m²s. Each curve given by the model presents the same shape as that given by the experiment.

As shown in Fig. 9 and for a low heating power P=1419W, the model results fit well the experimental results with a discrepancy smaller than 5%. However, the

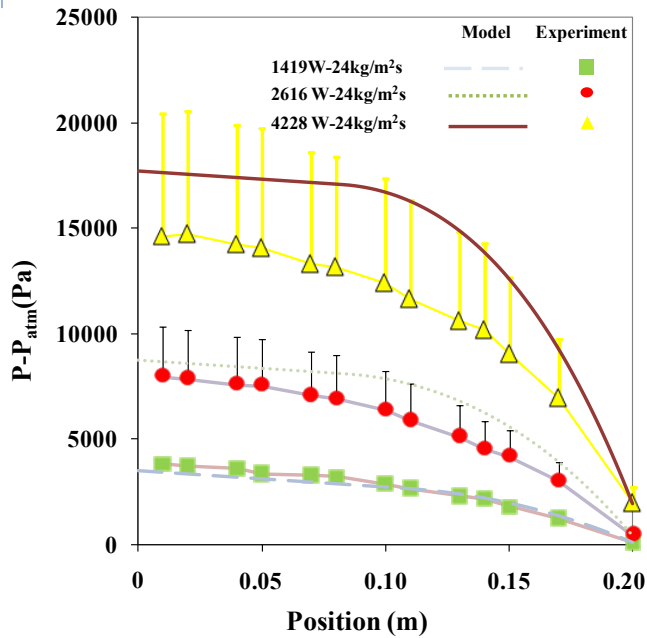


Figure 9: Experimental pressure loss compared to results obtained using homogeneous model for several heating power values.

discrepancy between the results given by the model and the experiments is noticeable, when the heating power is increased. For heating power values of 2226 W and 4225 W, the discrepancies are about 30% and 40% respectively. Note that the error bars in this figure which are drawn for each experiment point represent the maximum discrepancy in percentage between the experiment and the model.

The experimental results concerning the pressure loss *versus* modelling results are given in Fig. 10 for three heating power values: low (2616 W), high (4224 W) and intermediate (3425 W). Moreover, the maximum discrepancy between the two results is also represented in percentage for each point. As we can see in the figure, the global trend in the modelling results agrees quite well with the experiments. In particular, the increase of the pressure loss with velocity, followed by a decrease to reach the single-phase curve (as seen experimentally) is clearly reproduced by the model. For a low power value ($P=2616$ W), the model fits well the experiments. The discrepancy is about 2%, for a mass velocity varying in the range 35-50 kg/m²s. However, for this power and a mass flux less than 30 kg/m²s, the discrepancy between the two results is higher, about 20%. For the other two heating power values, there is a systematic discrepancy between experiments and modelling: 20% for $P=$

3425 W and 30% for P=4225W.

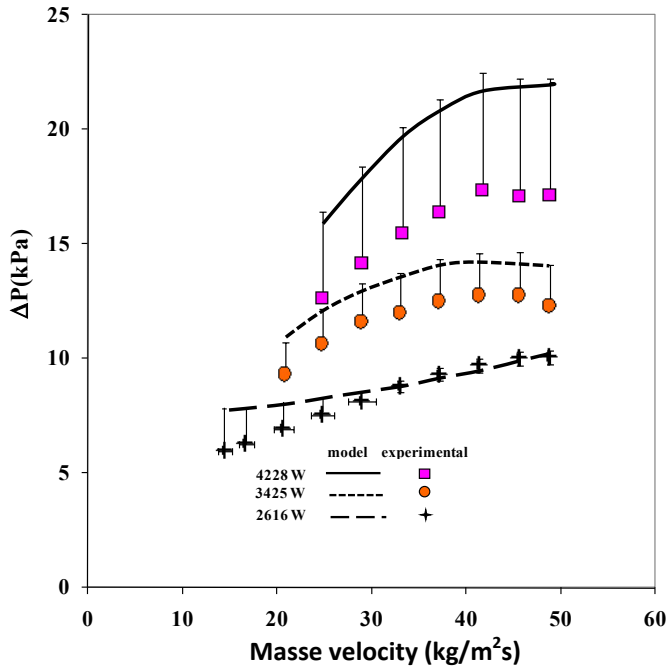


Figure 10: Experimental pressure loss *versus* mass velocity compared to results given by homogeneous model.

Figure 11 can be used to give a physical explanation to what happens. The figure provides both pressure loss and vapor mass quality *versus* mass flux for a heating power value P=2616W. The modelling results depend strongly on the exit vapor mass quality. For x values between 18% and 35%, the two-phase flow homogenous model accurately describes the experimental results. The discrepancy between the two results doesn't exceed the experimental uncertainty, which is approximately 2%. However, for x in the range 35% to 80%, the discrepancy between the results increases from 3% to 20%.

The good fit of experimental and model results for both low heating power and low mass vapor quality is certainly due to the flow structure which should be bubbly under these operating conditions. Hence, the assumption of homogeneous mixture of vapour-liquid seems correct. The relatively high discrepancy between modelling and experimental results for high heating power values is also due to the flow structure. The vapour mass quality in this case is up to 35%, which indicates that the flow structure passes from bubbly to slug pattern. As a consequence the hypothesis

of homogeneous mixture is not valid. However, the use of the actual mass quality profile which lacks in this study for the adopted model, is expected to lower the discrepancy.

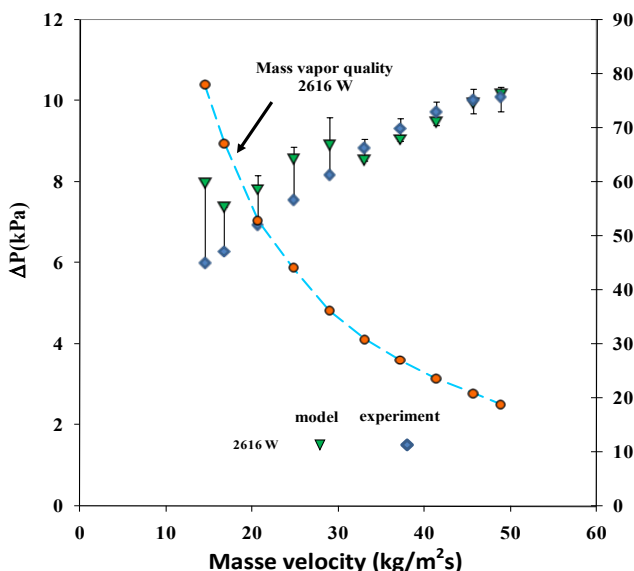


Figure 11: Pressure loss (model and experiment) and mass quality *versus* mass velocity for heating power P=2616W.

4 Conclusion

The present study is among the first works on the experimental analysis of convective boiling flow laws in a channel provided with metallic foam. The objective of the work is, on the one hand to get a better understanding of convective boiling in porous media and especially in cellular material and on the other hand to provide manufacturers of compact heat and mass exchangers with highly demanded refined data about this type of material.

To obtain a reliable database, special attention was paid to the choice of the various components of the experimental set up. The inlet liquid flow rate, the heating power and the inlet liquid temperature are the input data parameters, while the local static pressure, the distribution of temperature in the channel, and the exit mass quality constitute the output data.

The distribution of the local static pressure in the test section has been established for several mass velocities. The measured curves clearly show the effect of the

acceleration of the fluid due to phase change, and allow the determination of the boiling front with sufficient accuracy for different working conditions. The flow laws consist of a set of curves which represent the pressure gradient *versus* mass velocity for several heating power values. The results clearly show that the laws governing flow in a channel provided with metallic foams are very similar to those for a devoid channel.

The experimental results encouraged us to test models usually considered for two-phase flow in clear tube using the present database. Only the homogenous model for two-phase flow in clear tube is considered due to the fact that this model assumes the same velocity for each phase. The results of the comparison show that this model is relevant only for low heating power values. In this case the discrepancy between modelling and experiments is equal to the measurement uncertainty magnitude, which is about 2%. Note that the same conclusion has been established in a previous work only for convective boiling in a sintered fibrous channel (Miscvic, 1997) with porosity smaller than the porosity of metallic foam.

References

- Bhattacharya, A.; Calmidi, V. V.; Mahajan, R. L.** (2002): Thermophysical properties of high porosity metal foams. *International Journal of Heat and Mass Transfer*, Vol. 45, pp. 1017-1031.
- Bastarows, A. F.; Evans, A. G.; Stone, H. A.** (1998): Evaluation of cellular metal heat dissipation media. *Technical report MECH-325*, DEAS, Harvard University.
- Bau H.H.; Torrance K. E.** (1982): Boiling in low-permeability porous materials. *International Journal of Heat and Mass Transfer*, Vol. 25, No. 1, pp. 45- 55.
- Boomsma, K.; Poulikakos, D.** (2002): The effects of compression and pore size variations on the liquid flow characteristic in metal foams. *Journal of fluids engineering, Transactions of the ASME*, Vol. 124, pp. 263-272.
- Bonnet, J. P.; Topin, F.; Tadrist, L.** (2008): Flow laws in metal foams: compressibility and pore size effects. *Transport in Porous Media*, Vol. 73, pp. 233-254.
- Calvo, S.; Beugre, D.; Crine, M.; Léonard, A.; Marchot, P.; Toye, D.** (2009): Phase distribution measurements in metallic foam packing using X-ray radiography and micro-tomography. *Chemical engineering and processing: Process intensification*, Vol. 48, pp.1030-1039.
- Carey, V. P.** (1992): *Liquid vapor phase change phenomena: an introduction to the thermophysics of vaporization and condensation processes in heat transfer equipment*, Hemisphere Publishing Corporation.
- Chung, M.; Catton, I.** (1988): Multi-dimensional two-phase flow in porous media

with phase change. *AIChE Symposium*, Series 263, Vol. 84, pp. 177-185.

Collier J. C. (1972): *Convective boiling and condensation*. Mc Graw Hill, Book Company.

Curran, D. C. (2003): *Aluminium foam production using calcium carbonate as a foaming agent*. PHD dissertation, University of Cambridge.

Fukusako, S.; Komoriya, T.; Seki, N. (1986): An experimental study of transition and film boiling heat transfer in liquid-saturated porous bed. *Transactions of the ASME, Journal of Heat Transfer*, Vol. 108, pp. 117-124.

Hetsroni G. (1982): *Handbook of multiphase systems*. Hemisphere Publishing Corporation, Washington.

Jamialahmadi, M.; Müller-Steinhagen, H.; Izadpanah, M. R. (2005): Pressure drop, gas hold-up and heat transfer during single and two phase flow through porous media. *International Journal of Heat and Fluid Flow*, Vol. 26, pp. 156-172.

Kaviany, M. (1991): *Principles of heat transfer in porous media*. Springer-Verlag.

Kaviany, M.; Mittal, M. (1987): Natural Convection heat transfer from a vertical plate to high permeability Porous media: An experiment and an approximate solution. *International Journal of heat and mass transfer*, Vol. 30, pp. 967-977.

Kovalev, S. A.; Solov'yev, S. L.; Ovodkov, O. A. (1987): Liquid boiling on porous surfaces. *Heat transfer-soviet research*, Vol. 19, no. 3.

Liao, Q.; Zhao, T. S. (2000): A visual study of phase-change heat transfer in a two-dimensional porous structure with a partial heating boundary. *International Journal of Heat and Mass Transfer*, Vol. 43, pp. 1089-1102.

Lipinski, R. J., (1980): A particulate bed dryout model with upward and downward boiling. *Transaction of the American Nuclear Society*, Vol. 35, pp. 358-360.

Madani, B. (2007): *Etude expérimentale des écoulements et de l'ébullition dans les milieux poreux cellulaires*. PHD dissertation, USTHB, Algiers.

Madani, B.; Topin, F.; Rigollet, C.; Tadrist, L. (2007): Flow laws in metallic foams: Experimental determination of inertial and viscous contributions. *Journal of porous media*, Vol. 10 (1), pp. 51-70.

Mahjoob, S.; Vafai, K. (2008): A synthesis of fluid and thermal transport models for metal foam heat exchangers. *International Journal of Heat and Mass Transfer*, Vol. 51, pp. 3701-3711.

Miscevic, M.; Topin, F.; Tadrist, L. (2002): Convective boiling phenomena in a sintered fibrous channel: Study of thermal non-equilibrium behavior. *Journal of Porous Media*, Vol. 5 (4), pp. 229-239.

Naik, A. S.; Dhir, V. K. (1982): Forced flow evaporative cooling of a volumet-

rically heated porous layer, *International Journal of Heat Transfer*, Vol. 25, pp. 541-552.

Nakayama, W.; Daikoku Kuwahara, H.; Nakajima, T. (1982): Effects of pore diameters and system pressure on saturated pool nucleate boiling heat transfer from porous surfaces. *Journal of Heat Transfer*, Transactions of the ASME, Vol. 104, pp. 286-291.

SCPS patents, no. 95.09547 (1995), no. 98.03375 (1998), no. 98.04547 (1998).

Stemmet, CP.; Jongmans, J. N.; Schaaf, J.; Kuster, B.F.M.; Schouten, J.C. (2005): Hydrodynamics of gas-liquid counter-current flow in solid foam packings. *Chemical Engineering Science*, Vol. 60, pp. 6422-6429.

Tadrist, L.; Miscovic, M.; Rahli, O.; Topin, F. (2004): About the use of fibrous materials in compact heat exchangers. *Experimental thermal and fluid science*, Vol. 28, pp. 193-199.

Topin, F.; Bonnet, J. P.; Madani, B.; Tadrist, L. (2006): Experimental Analysis of Multiphase Flow in Metallic foam: Flow Laws, Heat Transfer and Convective Boiling. *Advanced Engineering Material*, Vol. 8, No. 9, pp. 890- 899.

